Volume 16, Issue 4, 162420 (1-10)

Iranian Journal of Earth Science (IJES)

https://dx.doi.org/10.57647/j.ijes.2024.1604.20

A work flow for carbonate rock physics modeling: a log-base methodology

Isti Nur Kumalasari[1*], Ignatius Sonny Winardhi[2], Rahmat Catur Wibowo[1]

[1]*Geophysical Engineering, Engineering Faculty, Universitas Lampung, Bandar Lampung, Lampung, Indonesia.*
[2]*Exploration and Engineering Seismology Research Group, Faculty of Mining and Petroleum Engineering, Bandung Institute of Technology, Bandung, Indonesia.*

*Corresponding author: isti.nurkumalasari@eng.unila.ac.id

Review Paper

Received:
3 November 2023
Revised:
22 December 2023
Accepted:
26 January 2024
Published online:
15 July 2024

Abstract:

Rock physics modeling plays an important role in determining the character of carbonate reservoirs. Reservoir characterization in carbonate rocks is more complex because it has various types of pores. Pore type analysis is very important for considering the analysis of seismic data and also for considering the proper drilling technique. Pore type is generally estimated using thin section data, but thin section data is not always available. Thus, in this paper we introduce a rock physics modeling workflow in carbonate reservoirs using well log data. The well log data used in this study located in Kujung I Formation, East Java Basin. To get the right elastic property model of carbonate rock, the main thing that needs to be considered is the estimation of the mineral matrix modulus and the aspect ratio with various approaches. By using a modified Kumar and Han (2005) method, the aspect ratio of soft pore, reference pore, and stiff pore are 0.09, 0.177, and 0.506, respectively. The velocity modeling is done by using Kuster-Toksöz equation. The results of the elastic properties modeling are close to the actual data. The correlation between the Vp Kuster-Toksöz and the actual Vp are 0.9269. While the correlation between the Vs Kuster-Toksöz and the actual Vs are 0.9803.

Keywords: Rock physics modeling; Carbonate reservoir; Elastic properties; Pore type; Aspect ratio

1. Introduction

About 50% of oil and gas production are generated by carbonate reservoirs (Xu and Payne, 2009). Therefore elastic property modeling of carbonate reservoir is crucial for petroleum industry (Jouni et al., 2011). Rock physics modeling of carbonate rock is more complicated because it has a variety of pore geometries (Kuster and Toksoz, 1974; Berryman, 1980; Xu and White, 1995; Wang, 2001; Eberli et al., 2003; Rash and Sadeq, 2018; Sharifi, 2022; Durrani et al., 2023; Karimiazar et al., 2023). Rock physics modeling to identify pore types is an important step in the study of increasing well production because pore shapes are related to permeability and fluid flow (**Prananda2020**). General method for identifying pore types is thin section analysis but thin section data is not continuous for every depth and not always available. The results of studies using well log analysis show that this method is effective for characterizing reservoirs vertically (Cui et al., 2017; Mahmoud et al., 2017; Dehghan and Yazdi, 2023). Therefore, by using log data for the physical modeling of this rock, the pore type for each depth can be generated (Dou et al., 2011; Hutami and Sudarsana, 2019). Therefore, this journal aims to elucidate a workflow for rock physics modeling in carbonate reservoir based on well log mathematical process.

Pore shapes have an important role in carbonate (Lubis and Harith, 2014). Heterogeneous pore shapes in carbonate rocks can be represented by the aspect ratio parameter, so that a study on this matter needs to be carried out. In this study, a modified method of Kumar and Han (2005) was used to predict the aspect ratio using the Wyllie time average equation, the Hashin-Shtrikman upper bound, and the Hashin-Shtrikman lower bound as representations of each pore type. In this study Kuster-Toksöz approach is used to calculate the effective modulus of carbonate rock. The result of exact elastic property value will be integrated with other data to determine reservoir character information in future studies.

2. Geological setting

The research area is located in the Kujung I Formation, East Java Basin (Figure 1). The East Java Basin is a backward arc basin at the southeast edge of stable Sundaland exposure. Bemmelen (1949) divides the North East Java Basin based on physiography into three zones, namely the Kendeng Zone, the Randublatung Zone, and the Rembang Zone. The research area is located in the Rembang zone. Based on the stratigraphic structure at the age of Oligocene, in the east there was a sea level increase which resulted in the deposition of the limestone of the Prupuh Formation and the Kujung Formation. The Kujung Formation consists of sandstone, limestone, shale, and marl (Mudjiono and Pireno, 2001). The Kujung Reservoir is sealed by a claystone from the Tuban Formation with a thickness of 500 to 1500 ft. The Kujung Formation is divided into 3 parts, namely the Kujung I Formation, Kujung II Formation, and Kujung III Formation. The Kujung 1 Formation is dominated by coral limestone. The thickness of Kujung I formation depends on local reef development.

3. Theory

3.1 Carbonate rocks

Carbonate rocks have complex pore systems such as vuggy, interparticle, moldic, and intraparticle. This complexity causes the relationship between porosity and velocity to be very scattered. Eberli et al. (2003) indicated that the pore type caused a 43% change in the velocity of the P-wave. The velocity of S-waves is predominantly influenced by the pore type (pore shape), especially oblate pores or cracks (Wang et al., 2009). Small or thin pores such as micro porosity and cracks cause a decrease in seismic wave velocity due to softening of the rock. Meanwhile, porosity with a large round shape, such as vuggy porosity, makes the rock stronger and causes an increase in seismic wave velocity compared to interparticle porosity (Xu and Payne, 2009). Classification of pore types in carbonate rocks in rock physics is divided into three (Figure 2), namely soft pore with a low aspect ratio value (microporosity or crack), reference pore with a medium aspect ratio value (interparticle or intercrystalline pore), and stiff pore with an aspect ratio higher (vuggy or moldic porosity). Carbonate rocks that have both reference and stiff pore types will have higher P-waves values than rocks with only reference pore types. Meanwhile, carbonate rocks that have both reference and soft pore types will have lower P-waves values compared to rocks with only reference pore pore types.

3.2 Rock physics analysis

Each type of pore has a certain aspect ratio (α). Aspect Ratio (Figure 3) is the ratio between the shortest ellipsoid axis (2a) and the longest axis (2c) (Xu and Payne, 2009; Schon, 2011). The greater the aspect ratio value of a rock, the rounder the shape of the rock's pores and vice versa.
In practice, a three-pore type model is usually sufficient. The pore shape of the rock can be predicted using modified Kumar and Han (2005) method by determining the bounds using the Wyllie time average equation (reference pore), Hashin-Shtrikman upper bound (stiff pore), and Hashin-Shtrikman lower bound (soft pore). Kuster-Toksöz is a method for calculating the effective modulus of various types of inclusion in carbonate rock. The bulk and shear modulus ($K^{*}{}_{KT}$ and $\mu^{*}{}_{KT}$) equation of this method can be written as (Kuster and Toksoz, 1974; Berryman, 1980).

$$(K^*_{KT}-K_m)\frac{(K_m+\frac{4}{3}\mu_m)}{(K^*_{KT}+\frac{4}{3}\mu_m)}=\sum_{i=1}^{N}xi(K_i-K_m)P^{mi} \quad (1)$$

$$(u^*_{KT}-\mu_m)\frac{(\mu_m+\zeta_m)}{(\mu^*_{KT}+\zeta_m)}=\sum_{i=1}^{N}xi(\mu_i-\mu_m)Q^{mi} \quad (2)$$

where the summation is over the different inclusion types with volume concentration xi, P^{mi} and Q^{mi} are geometric

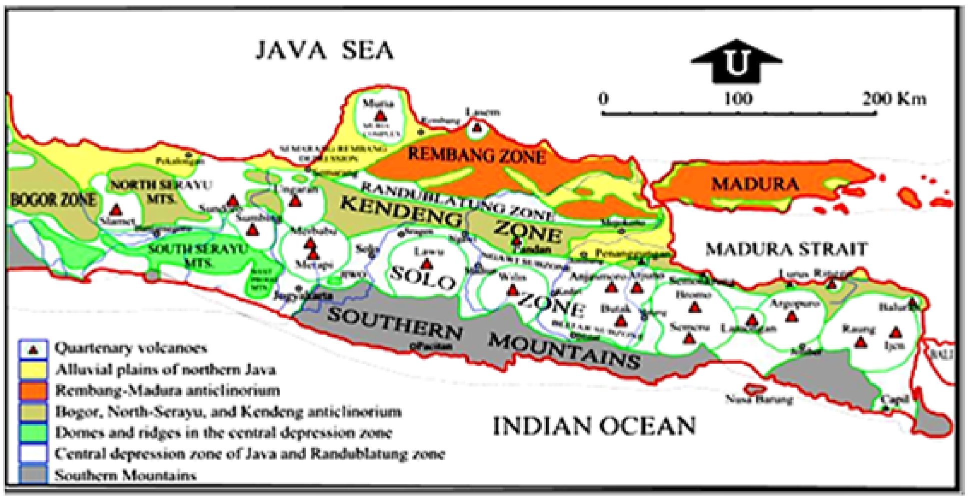

Figure 1. Physiographic zones of Java (Bemmelen, 1949).

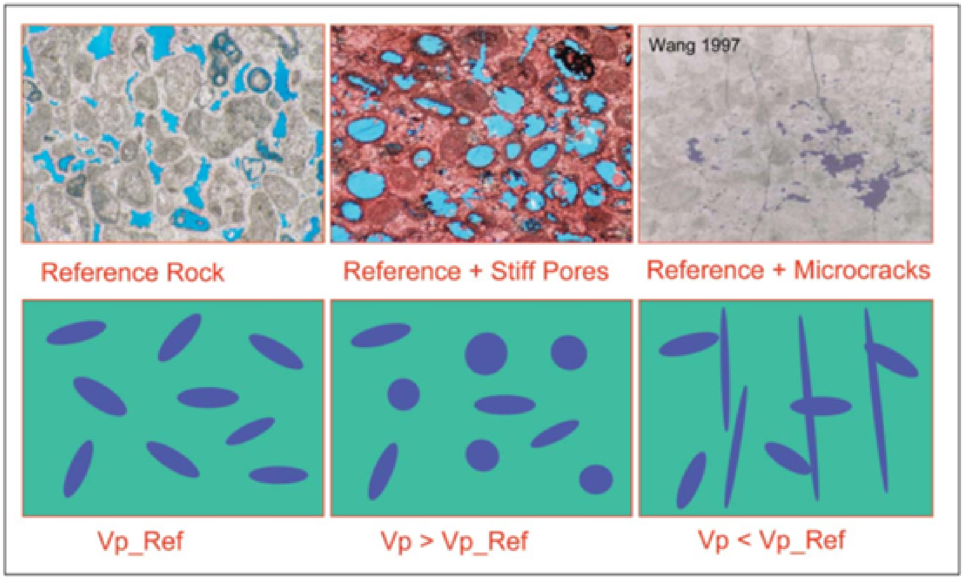

Figure 2. Carbonate pore types (Xu and Payne, 2009).

factor (Berryman, 1995), K_m is the bulk modulus of mineral, μ_m is the shear modulus of mineral, K_i is the bulk modulus of inclusion, μ_i is the shear modulus of inclusion.

4. Data and methodology

The data used in this study were well log data and petrophysical data. The availability daya on IN-2 wells consist of density, gamma ray, neutron porosity, volume of clay, total porosity (PHIT), effective porosity (PHIE), water saturation (Sw), P-wave (Vp), and S-wave (Vs).
The modeling of elastic properties in this study was carried out using the Kuster-Toksoz equation. Availability of petrophysical data has an important role to produce appropriate rock physics modeling. The more complete the data availability, the better rock physics modeling will be. There are several assumptions used in this study due to the unavailability of some supporting data. In this study there were some unspecified supporting data (XRD, temperature, pressure, salinity, oil gravity, and GOR), so several assumptions were needed in this rock physics modeling. The workflow of the rock physics modeling is shown in Figure 4.

4.1 Data elimination

Before carrying out the processing of rock physics model, we need to eliminate data on the target zone which has a clay volume value more than 0.2 (Figure 5). Zhao et al. (2013) stated that the clay content causes perturbation in P-wave velocity. This is done so that the modeling focuses on carbonate rocks, so we need to minimize the effect of claystone.

4.2 Estimation of the elastic modulus of fluids

The estimation of the elastic modulus of the fluid is carried out using Wood's equation (Wood, 1995). The elastic parameters of the pore-filling fluid used are $K_{\text{brine}} = 2.20$ GPa, $K_{\text{gas}} = 0.2$ GPa, $\rho_{\text{brine}} = 1$ g/cc, $\rho_{\text{gas}} = 0.001$ g/cc, due to the absence of data on pressure, temperature and salinity, it is necessary to assume the values of these parameters.

4.3 Determination of initial bulk modulus and shear modulus of solid rock

Due to the limited XRD data, the initial solid rock elastic modulus estimation was carried out by making a crossplot between the K_{sat} data against total porosity in the wet zone data (Kujung I). The initial K_{min} value is estimated by looking at K_{sat} curve trend at zero porosity and the same way was done to estimate initial μ_{min} value. This is because the value of K and μ in rock conditions with zero porosity are considered the same as solid rock. Figure 6 is a crossplot between bulk modulus and shear modulus against total porosity. The trendline show the best fitting equation and the curve trend at zero porosity. Kmin and min are obtained by inputting a porosity value of zero ($x = 0$) to the equation.
Y (K_{sat}) = $536.47(X^2) - 321.65(X) + 63.908$

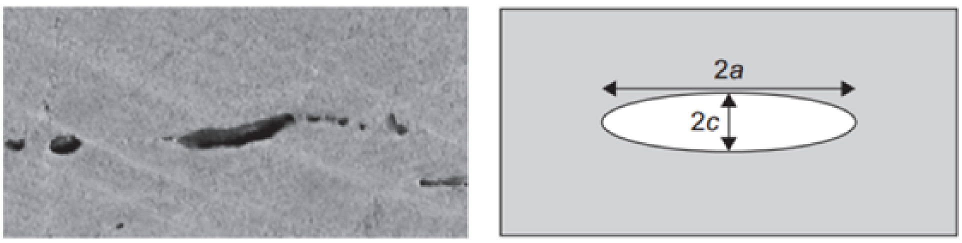

Figure 3. Aspect Ratio Ilustration $\alpha = c/a$ (Schon, 2011).

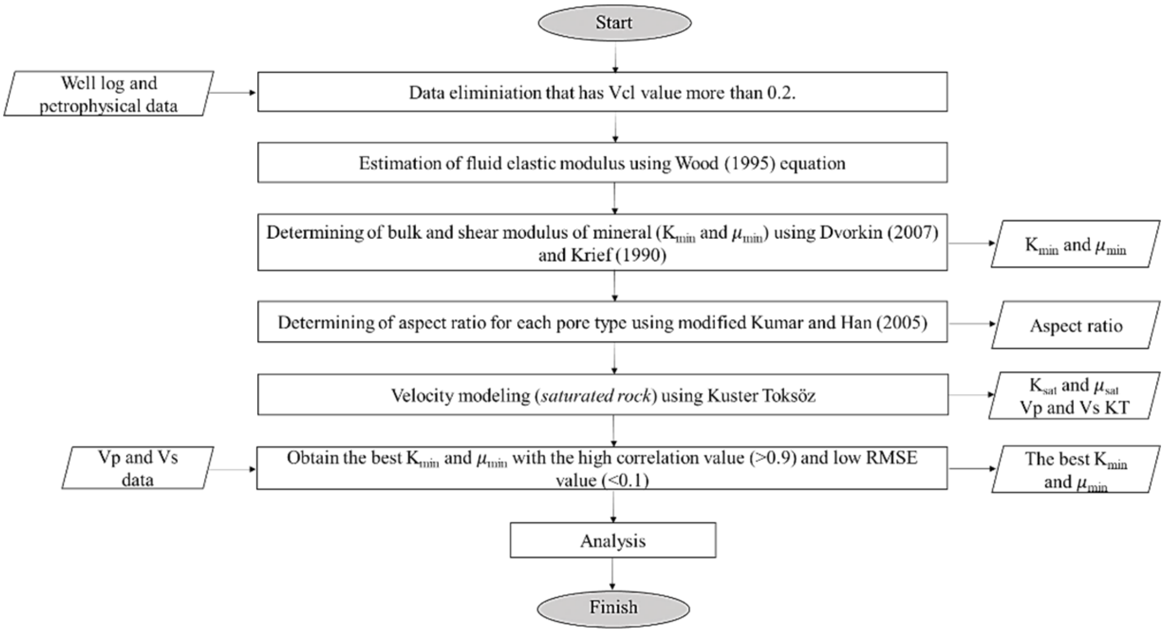

Figure 4. Rock physics modeling flowchart.

Y (K_{sat} at total porosity porosity 0) $= 536.47(0^2) - 321.65(0) + 63.908$
Y (K_{sat} at total porosity porosity 0) $= 0 - 0 + 63.908$
Y (K_{sat} at total porosity porosity 0) $= 63.908$
Y (K_{sat} at total porosity porosity 0) $= 64$ (rounding values up)
By using the same methode we obtained the $\mu_{min} = 26$ GPa.

The initial K_{min} and and μ_{min} value is assumed as a K_{sat} and μ_{sat} value at zero porosity. Therefore, K_{min} value is 64 GPa and μ_{min} value is 26 GPa.

To predict K_{min} and μ_{min} for each depth can be done using the Dvorkin (2007) and Krief et al. (1990) equations. K_{min} prediction is done using the Krief equation below (Equa-

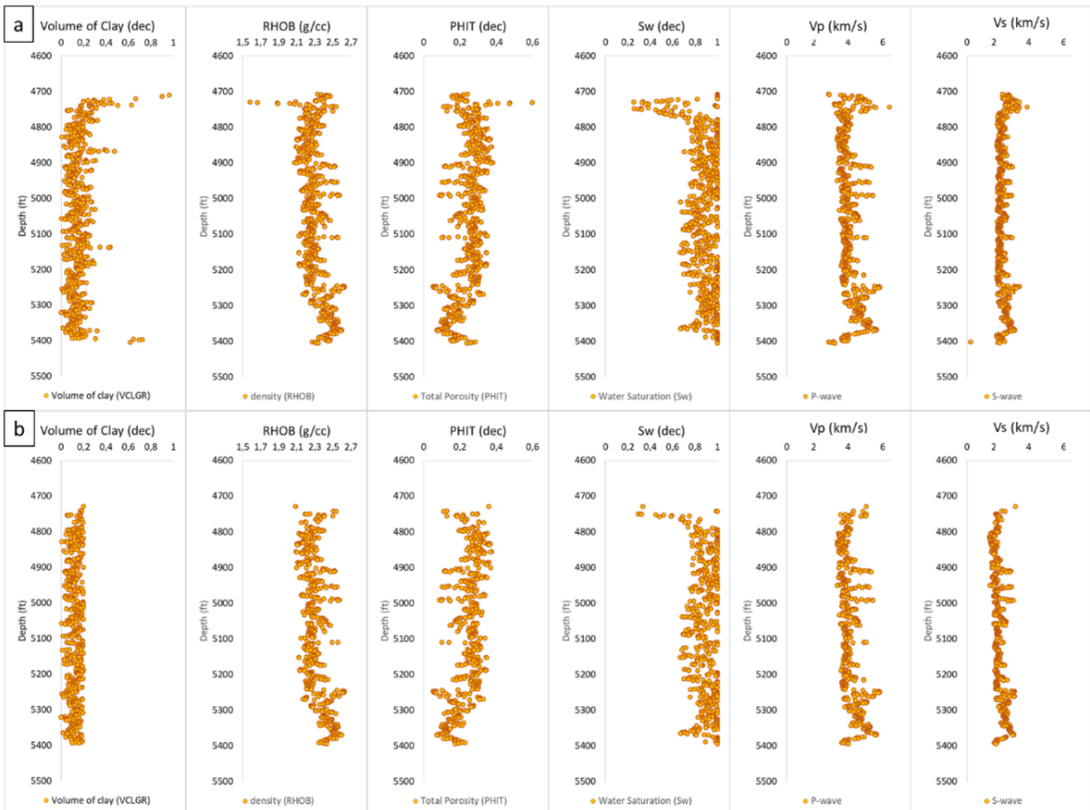

Figure 5. (a) Well log data before elimination (b) Well log data after elimination (Vcl >0.2).

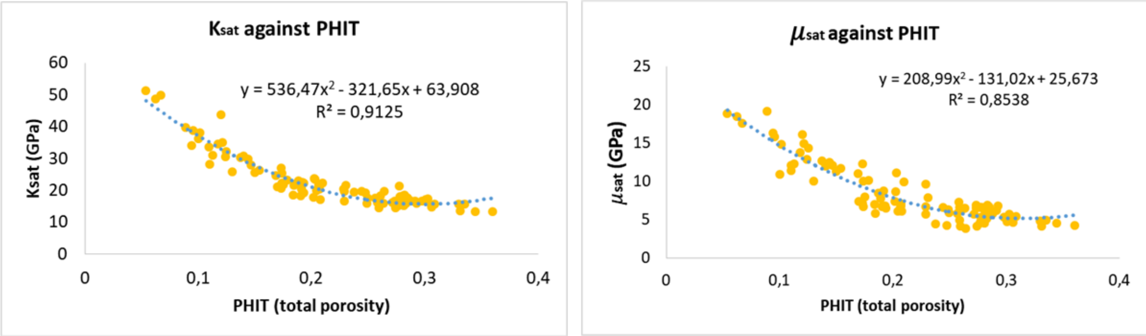

Figure 6. Initial estimation of $K_{\min}$ and $\mu_{\min}$.

tions (3) and (4)),

$$K_{\text{dry}} = K_{\text{ma}}(1-\varphi)^{m(\varphi)} \tag{3}$$

$$\mu_{\text{dry}} = \mu_{\text{min}}(1-\varphi)^{m(\varphi)} \tag{4}$$

$$m(\varphi) = \frac{3}{(1-\varphi)} \tag{5}$$

μ_{min} prediction is done using μ_{sat} data because μ_{sat} is the same as μ_{dry}. Before calculating K_{min}, we need to first calculate K_{dry} with the inverse Biot Gassmann equation.

$$K_{sat} = K_{dry} + \frac{(1-\frac{k_{dry}}{k_{min}})^2}{\frac{\varphi}{k_{fl}} + \frac{1-\varphi}{k_{min}} - \frac{k_{dry}}{k_{min}^2}} \tag{6}$$

$$\mu_{sat} = \mu_{dry} \tag{7}$$

Below are the flow steps of predicting K_{min} and μ_{min} for each depth using Krief equation:
1. Before calculating the the μ_{min}, we need to calculate μ_{dry} value. Because μ_{sat} is the same as μ_{dry}, use the following equation:

$$V_s = \sqrt{\frac{\mu_{sat}}{\rho}} \tag{8}$$

Then calculate the μ_{min} using the following equation:

$$\mu_{dry} = \mu min(1-\varphi)^{m(\varphi)} \tag{9}$$

$$m(\varphi) = \frac{3}{1-\varphi} \tag{10}$$

where Vs is log data of S-wave, ρ is the log data of RHOB, and φ is total porosity data
2. Calculate K_{sat} using the following equation:

$$V_p = \sqrt{\frac{k_{sat} + \frac{4}{3}\mu_{sat}}{\rho}} \tag{11}$$

where Vp is log data of P-wave, ρ is the log data of density, and μ_{sat} is saturated modulus from previous calculation. The calculation of K_{dry} was done by using inverse Biot Gassman equation (Gassmann, 1951) bellow:

$$K_{sat} = K_{dry} + \frac{(1-\frac{k_{dry}}{k_{min}})^2}{\frac{\varphi}{k_{fl}} + \frac{1-\varphi}{k_{min}} - \frac{k_{dry}}{k_{min}^2}} \tag{12}$$

The next step is calculating the K_{min} using Krief equation bellow:

$$K_{dry} = K_{min}(1-\varphi)^{m(\varphi)} \tag{13}$$

Predict K_{min} and μ_{min} using the Dvorkin equation below:

$$Vp = Vp_{dry} + \varphi Vp_f \tag{14}$$

$$Vp_{dry} = (1-\varphi)^2 Vp_s \tag{15}$$

$$Vs_{dry} = (1-\varphi)^2 Vs_s \tag{16}$$

$$Vs = Vs_{dry}\sqrt{\frac{\rho_{dry}}{\rho_b}} \tag{17}$$

$$\rho_b = (1-\varphi)\rho_s + \varphi\rho_f \tag{18}$$

$$\rho_{dry} = (1-\varphi)\rho_s \tag{19}$$

Before estimating K_{min} and μ_{min} for all depth, ρ_{matrix} and ρ_{water} were carried out in the wet zone ($S_w = 1$). From the wet zone data, a fitting is made to the density data to get the best ρ_{matrix} and ρ_{water}. The best fitting equation of the density and total porosity crossplot is used to determine the rho matrix. The rho matrix is assumed to have the same value as the density when the porosity value is zero. The density porosity equation on Figure 7 show that $\rho_{matrix} = 2.7193$ g/cc.
The ρ_{water} value is predicted using the bulk density equation and the ρ_{matrix} value from previous estimation. From the bulk density equation, find the best ρ_{water} value by comparing the calculated bulk density to the actual bulk density (RHOB). Figure 8 show that the bulk density calculation match to the actual data. The ρ_{matrix} and ρ_{water} values are used to predict K_{min} and μ_{min} for all depths using Dvorkin

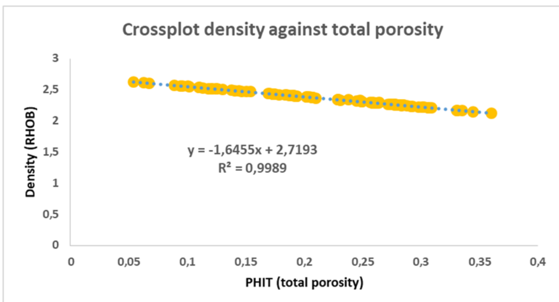

Figure 7. Crossplot density against total porosity.

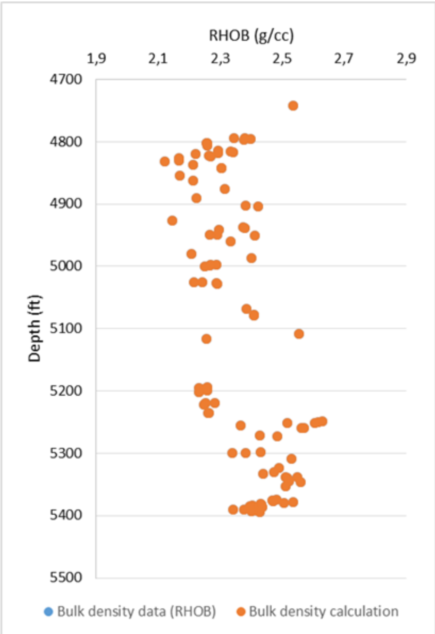

Figure 8. Comparison of calculated bulk density and measured bulk density.

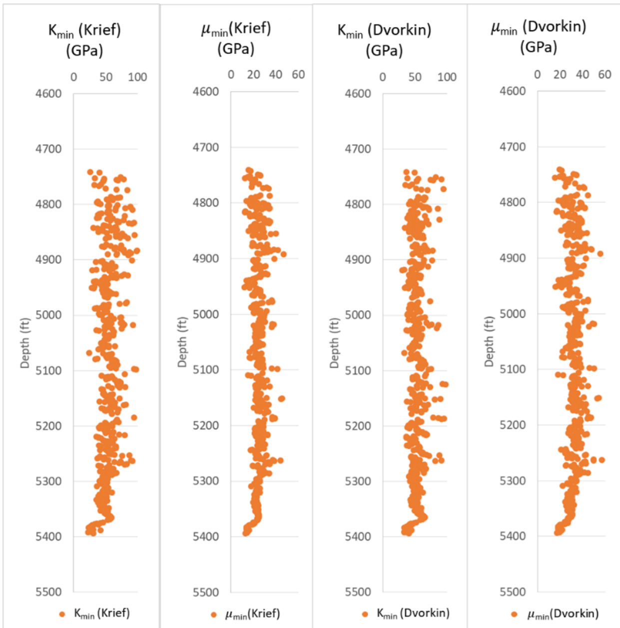

Figure 9. K_{min} and μ_{min} calculation.

equation. Figure 9 show the result of K_{min} and μ_{min} calculation using Dvorkin and Krief equation for each depth.

$$\mu_{min} = \frac{Vs_s}{\rho_{matrix}} \tag{20}$$

$$K_{min} = Vp_s^2 \times \rho_{matrix} - \frac{4}{3}\mu_{min} \tag{21}$$

4.4 Aspect ratio determination

The aspect ratio value in this study was estimated using a modified method of Kumar and Han (2005). Before determining the aspect ratio, it is necessary to separate the wet zone and saturated gas data. Because the aspect ratio prediction is based on P-wave data (Vp), if the data is treated the same it lead to mispredictions. The steps for determining the aspect ratio are:
1. Calculate the *Vp* value using Wyllie time-average (Wyllie et al., 1958) equation from available porosity data dari data (for reference pore).
2. Calculate the *Vp* value using Hashin-Shtrikman upper bound equation (Hashin and Shtrikman, 1963) from available porosity data (for stiff pore).
3. Calculate the *Vp* value using Hashin-Shtrikman lower bound equation (Hashin and Shtrikman, 1963) from available porosity data (for soft pore).
4. Calculate the *Vp* value using Kuster- Toksöz (KT) equation from available porosity data with an initial aspect ratio of 0.01 for soft pore, 0.1 for reference pore, dan 1 for stiff pore. Find the best aspect ratio which has the lowest error of calculated *Vp* data for each *Vp* Hashin-Shtrikman lower bound (soft pore), *Vp* Wyllie time-average for reference pore, *Vp* Hashin-Shtrikman upper bound for stiff pore.
5. If $(VP, KT(\alpha) - Vp(\alpha))^2 > \varepsilon$ then $\alpha = \alpha \pm \delta\alpha$. Determine the best aspect ratio by comparing *Vp* calculated by Kuster-Toksöz againts *Vp* Hashin-Shtrikman lower bound (soft pore), *Vp* Wyllie time-average for reference pore, and *Vp* Hashin-Shtrikman upper bound for stiff pore. If the error results obtained are not yet minimum, the aspect ratio (α) needs to be increased and decreased (by the smallest alpha part (δ)) until the smallest error is obtained (ε).
6. Use the aspect ratio of each pore type if $((VP, \text{KT}(\alpha) - Vp(\alpha))^2 < \varepsilon$. The aspect ratio of each pore type is the aspect ratio that produces *Vp* Kuster-Toksöz with the smallest error (ε) compared to the actual *Vp*.
7. Obtain the aspect ratio of each pore type (Figure 10).

After we get each aspect ratio of pore type, it is a necessary to find the fraction of each pore type (Figure 10). The calculation of the soft pore fraction and reference pore for data located between *Vp* Wyllie and *Vp* Hashin-Shtrikman lower bound is as follows:

$$\text{Soft pore fraction} = \frac{(Vp\ \text{Wyllie} - Vp\ \text{data})}{(Vp\ \text{Wyllie} - Vp\ \text{HS lower boun})} \tag{22}$$

$$\text{Reference pore fraction} = \frac{(Vp\ \text{data} - Vp\ \text{HS lower bound})}{(Vp\ \text{Wyllie} - Vp\ \text{HS lower bound})} = 1 - \text{soft pore fraction} \tag{23}$$

The calculation of the stiff pore fraction and reference pore for data located between *Vp* wyllie and *Vp* Hashin-Shtrikman upper bound is as follows:

$$\text{Soft pore fraction} = \frac{(Vp\ \text{data} - Vp\ \text{Wyllie})}{(Vp\ \text{HS upper bound} - Vp\ \text{Wyllie})} \tag{24}$$

$$\text{Reference pore fraction} = \frac{(Vp\ \text{HS upper bound} - Vp\ \text{data})}{(Vp\ \text{HS upper bound} - Vp\ \text{Wyllie})} = 1 - \text{stiff pore fraction} \tag{25}$$

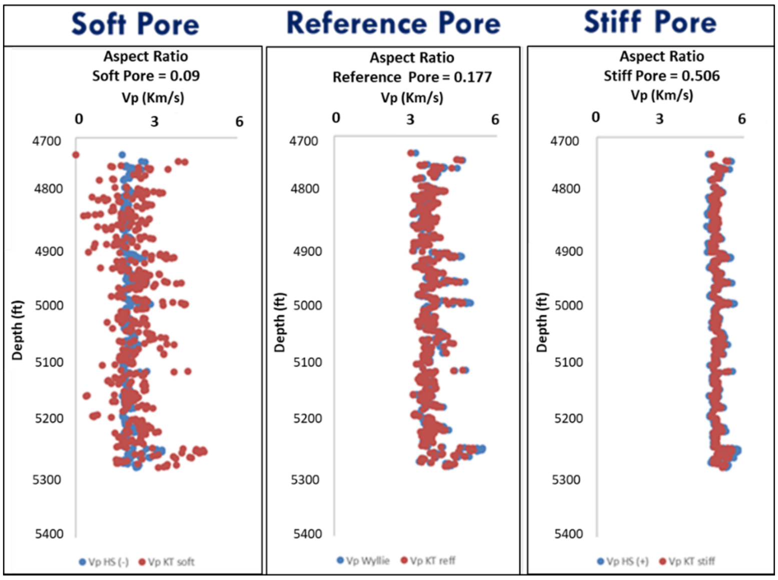

Figure 10. Determination of aspect ratio by using modified Kumar and Han (2005).

4.5 Velocity modeling (kuster-toksöz equation)

After the required elastic parameters have been obtained, the next step is inclusion modeling using Kuster-Toksöz to get the K_{sat} and μ_{sat} values. In this modeling, P_{mi} and Q_{mi} used are penny crack pores (Table 1). Inverse Wood (1995) equation used to calculate the modulus bulk of inclusion (K_i).

$$\beta = \mu_{min} \frac{(3K_{min} + \mu_{min})}{(3K_{min} + 4\mu_{min})} \quad (26)$$

$$\gamma = \mu_{min} \frac{(3K_{min} + \mu_{min})}{(3K_{min} + 7\mu_{min})} \quad (27)$$

$$\zeta = \frac{\mu_{min}}{6} \frac{(9k_{min} + 8\mu_{min})}{(k_{min} + 2\mu_{min})} \quad (28)$$

$$P_{mi} = \frac{(K_{min} + \frac{4}{3}\mu_i)}{(K_{min} + \frac{4}{3}\mu_i + \pi\alpha\beta_m)} \quad (29)$$

$$Q_{mi} = \frac{1}{5} \times \left(1 + \frac{8\mu_{min}}{(4\mu_i + \pi\alpha(\mu_{min} + 2\beta_{min})} + 2\frac{(K_i + \frac{2}{3}(\mu_i + \mu_{min})}{(K_i + \frac{4}{3}\mu_i + \pi\alpha\beta_{min})}\right) \quad (30)$$

$$\mu_i = 0 \quad (31)$$

$$K_i = \left(\frac{S_w}{K_{water}} + \frac{1 - S_w}{K_{hc}}\right)^{-1} \quad (32)$$

The K_{sat} and μ_{sat} values are calculated using Equation (1) and (2). To test the accuracy of the predicted elastic property values used in the modeling are correct, we need to compare the measured Vp dan Vs against the estimated results using the equation bellows:

$$Vp_{sat} = \sqrt{\frac{K_{sat} + \frac{4}{3}\mu_{sat}}{\rho_{sat}}} \quad (33)$$

$$Vs_{sat} = \sqrt{\frac{\mu_{sat}}{\rho_{sat}}} \quad (34)$$

4.6 Mineral modulus of solid rock final estimation

The velocity model result are not yet fit. Therefore, it is necessary to estimate the values of K_{min} and μ_{min} for every depth using the pore fractions from the previous stages. The prediction of K_{min} and μ_{min} are done using looping process which produce the lowest error value between calculated Vp dan Vs against the actual data (Hilman and Winardhi, 2019).

5. Result discussions

By using a modified Kumar and Han (2005) method, the aspect ratio of soft pore, reference pore, and stiff pore are 0.09, 0.177, and 0.506, respectively (Figure 11).
To check the rock physics modeling results, we need to compare the actual log data with the modeled log data (Azeem

Table 1. P^{mi} and Q^{mi} of penny cracks (Berryman, 1995).

Inclusion shape	P^{mi}	Q^{mi}
Penny cracks	$\frac{(K_m + \frac{4}{3}\mu_i)}{(K_m + \frac{4}{3}\mu_i) + \pi\alpha\beta_m}$	$\frac{1}{5}\left(1 + \frac{8\mu_m}{4\mu i + \pi\alpha(\mu_m + 2\beta_m)} + 2\frac{(k_i + \frac{2}{3}(\mu_i + \mu_m)}{(k_i + \frac{4}{3}\mu_i + \pi\alpha\beta_m)}\right)$

Note: $\beta = \mu \frac{(3K+\mu)}{(3K+4\mu)}, \gamma = \mu \frac{(3K+\mu)}{(3K+7\mu)}, \zeta = \frac{\mu}{6} \frac{9k+8\mu}{(k+2\mu)}, \alpha =$ aspect ratio.

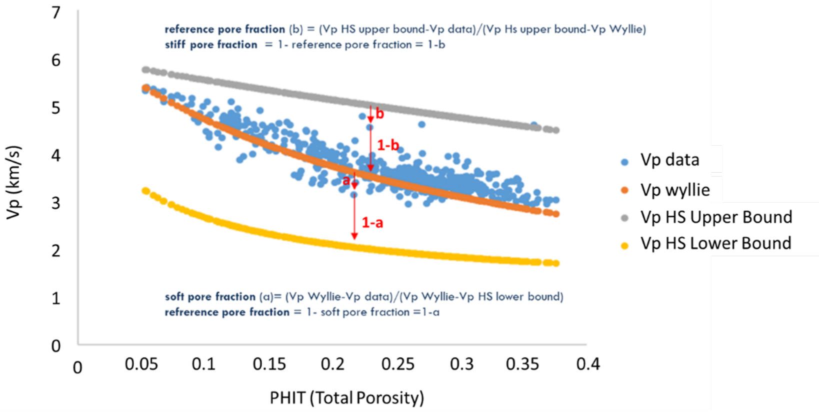

Figure 11. Illustration of pore fraction determination.

et al., 2017; Handoyo et al., 2019). This is important to ensure a high level of consistency to enable a single rock physics model.

A large aspect ratio value represents a stiff pore shape while a small aspect ratio value represents a softer pore shape. Data that is under the Wyllie time average equation calculation curve is considered to have a soft pore type, while data that is above the Wyllie time average curve is classified as having a stiff pore type. The Kujung 1 Formation is dominated by pore shape between the reference and stiff curves (87%). Meanwhile, the soft pore percentage (under the Wyllie time average curve) is 17%.

Figure 12 shows the result of elastic property modeling and the comparison between *Vp* and *Vs* modeling results against original data. Modeling results show a good match. The correlation and RMSE values between the *Vp* Kuster-Toksöz and the actual *Vp* are 0.9269 and 0.0719, respectively. While the correlation and RMSE values between the *Vs* Kuster-Toksöz and the actual *Vs* are 0.9803 and 0.0343, respectively. Based on the results of the elastic property modeling, the dominant aspect ratio value is around 0.17 to 0.19. These results indicate that the most likely pore type that develops in the Kujung I Formation is a reference pore. This research still has shortcomings because there is no validation of the results. To further increase the confidence in the prediction results of elastic properties that have been modeled, research on validating modeling results with thin section data needs to be carried out in future studies.

6. Conclusions

The main thing that needs to be considered to get the right elastic property model of carbonate rocks is the estimation of the mineral matrix modulus and aspect ratio with various approaches. The results of the elastic properties modeling are close to the actual data. The modeled *Vp* value has a high correlation with the original data *Vp* (0.9269) and the modeled *Vs* value has a high correlation with the original data *Vp* (0.9803). The RMSE value from the modeling results with the original data is less than 0.1.

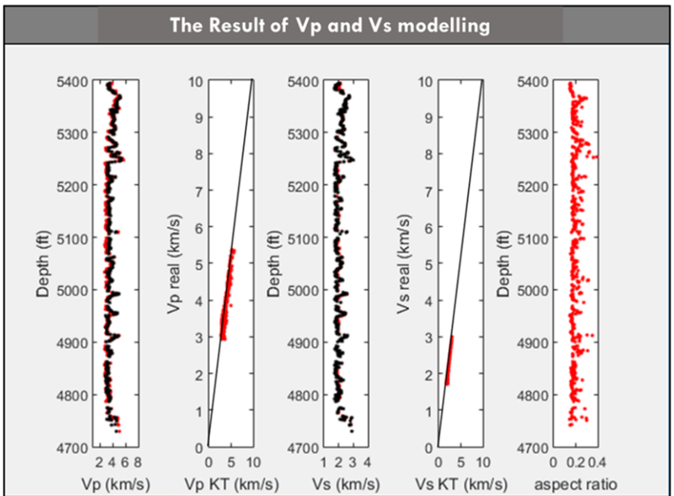

Kujung I Formation		Correlation	RMSE
	Vp	0.9269	0.0719
	Vs	0.9803	0.0342

Figure 12. The result of P-wave and S-wave velocity modeling using Kuster-Toksöz.

Acknowledgments
The authors would like to thank all those who have helped towards the entire process of drafting and publishing this paper especially Mr. Ignatius Sonny Winardhi, Ph.D and Exploration and Engineering Seismology Research Group, Faculty of Mining and Petroleum Engineering, Bandung Institute of Technology.

Authors contributions
All authors have contributed equally to prepare the paper.

Availability of data and materials
The data that support the findings of this study are available from the corresponding author upon reasonable request.

Conflict of interests
The authors declare that they have no known competing financial interests or personal relationships that could have appeared to influence the work reported in this paper.

References

Azeem T., Chun W. Y., Lisa M., Khalid P., Qing L. X., Ehsam M. I., Munawar M. J., Wei X. (2017) An integrated petrophysical and rock physics analysis to improve reservoir characterization of cretaceous sand intervals in middle indus basin, pakistan. *Journal of Geophysics and Engineering* 14:212–225. https://doi.org/10.1088/1742-2140/14/2/212

Bemmelen R. W. Van (1949) The geology of indonesia. vol. IA, general geology of indonesia and adjacent arhchipelagoes. netherlands. *Government Printing Office, The Hague*

Berryman J. G. (1980) Long-wavelength propagation in composite elastic media. *Journal of Acoustical Society of America* 68:1809–1831. https://doi.org/10.1121/1.385171

——— (1995) Mixture theories for rock properties. *American Geophysical Union,* 205–228. https://doi.org/10.1029/RF003p0205

Cui H., Zhong N., Li J., Wang D., Li Z., Hao A., Liang F. (2017) Study on the lower limit of petrophysical of the upper paleozoic tight sandstone gas reservoir in the ordoss basin, china. *Journal of Natural Gas Geoscience* 2:21–28. https://doi.org/10.1016/j.jnggs.2017.03.003

Dehghan A. N., Yazdi A. (2023) A geomechanical investigation for optimizing the ultimate slope design of shadan open pit mine, iran. *Indian Geotechnical Journal,* 1–15. https://doi.org/10.1007/s40098-022-00709-w

Dou Q., Sun Y., Sullivan C. (2011) Rock-physics-based carbonate pore type characterization and reservoir permeability heterogeneity evaluation, upper san andres reservoir, permian basin, west texas. *Journal of Applied Geophysics* 74 (1): 8–18. https://doi.org/10.1016/j.jappgeo.2011.02.010

Durrani M. Z. A., Rahman S. A., Talib M., Sarosh B. (2023) Discrimination of lithofacies in tight gas reservoir using field-specific rock physics modeling scheme. a case study from a mature field of middle indus basin, pakistan. *Acta Geophysica,* 1–18. https://doi.org/10.1007/s11600-023-01069-6

Dvorkin J. P. (2007) Yet another vs equation. *Geophysics* 73:35–39. https://doi.org/10.1190/1.2792795

Eberli G. P., Baechle G. T., Anselmetti F. S., Incze M. L. (2003) Factors controlling elastic properties in carbonate sediments and rocks. *The Leading Edge* 22:654–660. https://doi.org/10.1190/1.1599691

Gassmann F. (1951) Elasticity of porous media. *Uber Die Elastizitat Poroser Medien: Vierteljahrsschrift Der Naturforschenden Gesselschaft* 96:1– 23. https://doi.org/10.1190/1.9781560801931.ch3p

Handoyo, Fatkhan, Hutami H. Y., Sudarsana R. (2019) Rock physics model to determine the geophysical pore-type characterization and geological implication in carbonate reservoir rock. *IOP Conference Series: Earth and Environmental Science* 311 (1): 012031. https://doi.org/10.1088/1755-1315/311/1/012031

Hashin Z., Shtrikman S. (1963) A variational approach to the theory of the elastic behaviour of multiphase materials. *Journal of the Mechanics and Physics of Solids* 11 (2): 127–140. https://doi.org/10.1016/0022-5096(63)90060-7

Hilman J., Winardhi I. S. (2019) Rock physics template application on carbonate reservoir. *IOP Conference Series: Earth and Environmental Science* 318 (1): 012006. https://doi.org/10.1088/1755-1315/318/1/012006

Hutami H. Y., Sudarsana R. (2019) Rock physics model to determine the geophysical pore-type characterization and geological implication in carbonate reservoir rock. *IOP Conference Series: Earth and Environmental Science* 311 (1): 012031. https://doi.org/10.1088/1755-1315/311/1/012031

Jouni, Mohamed S., Vega S. (2011) Simulation of elastic properties in carbonate. *The Leading Edge,* 1400–1407. https://doi.org/10.1190/1.3672485

Karimiazar J., Teshnizi E. Sharifi, O'Kelly B. C., Sadeghi S., Karimizad N., Yazdi A., Arjmandzadeh R. (2023) Effect of nano-silica on engineering properties of lime-treated marl soil. *Transportation Geotechnics* 43:101123. https://doi.org/10.1016/j.trgeo.2023.101123

Krief M., Garat J., Stellingwerff J., Ventre J. (1990) A petrophysical interpretation using the velocities of p and s waves (full-waveform sonic). *The Log Analyst* 31 (6): 355–369.

Kumar M., Han D. (2005) Pore shape effect on elastic properties of carbonate rock. *SEG (Huston 2005 Annual Meeting),* 1477–1480. https://doi.org/10.1190/1.2147969

Kuster G. T., Toksoz M. N. (1974) Velocity and attenuation of seismic waves in two-phase media. *Geophysics* 39:587–618. https://doi.org/10.1190/1.1440450

Lubis L. A., Harith Z. Z. T. (2014) Pore type classification on carbonate reservoir in offshore sarawak using rock physics model and rock digital images. *IOP Conference Series: Earth and Environtmental Science* 19:012003. https://doi.org/10.1088/1755-1315/19/1/012003

Mahmoud M., Ghorab M., Shalzy T., Shibl A., Abuhagaza A. A. (2017) Reservoir characterization utilizing the well logging analysis of abu madi formation, nile delta, egypt, egyptian. *Journal of Petroleum* 26:649–659. https://doi.org/10.1016/j.ejpe.2016.11.003

Mudjiono, Pireno (2001) Exploration of the north madura platform offshore, east java indonesia. *Proceedings of the Indonesian Petroleum Association 28th annual Convention & Exhibition.,* https://doi.org/10.29118/ipa.980.707

Rash T. K., Sadeq Q. M. (2018) Development permeability prediction for bai hassan cretaceous carbonate reservoir. *UHD Journal of Science And Technology* 2:8–16. https://doi.org/10.21928/uhdjst.v2n1y2018.pp8-18

Schon J. H. (2011) Physical properties of rocks, a workbook, elsevier, netherland. 8:337–361.

Sharifi J. (2022) Multi-pore rock physics model: an intelligent approach for carbonate rocks. *Journal of Petroleum Science and Engineering* 218:1–12. https://doi.org/10.1016/j.petrol.2022.111002

Wang X., Zhang Y., Yan P., Liu L., Wang G., Li X., Wang X. (2009) Application of greenberg-castagna model in igneous rock region, seg technical program expanded abstract. 2233–2237.

Wang Z. J. (2001) Fundamentals of seismic rock physics. *Geophysics* 66 (2): 398–412. https://doi.org/10.1190/1.1444931

Wood A. B. (1995) A textbook of sound, third ed. the mcmillan co, new york. *Cambridge University Press:The Aeronautical Journal,* https://doi.org/10.1017/S0368393100130998

Wyllie M. R. J., Gregory A. R., Gardner G. H. F. (1958) An experimental investigation of factors affecting elastic wave velocities in porous media. *Geophysics* 23:459–493. https://doi.org/10.1190/1.1438493

Xu S., Payne M. A. (2009) Modeling elastic properties in carbonate rocks. *The Leading Edge,* 66–74. https://doi.org/10.1190/1.3064148

Xu S., White R. E. (1995) A new velocity for clay sand mixtures. *Geophysical Prospecting* 43:91–118. https://doi.org/10.1111/j.1365-2478.1995.tb00126.x

Zhao L., Nasser M., Han D. (2013) Quantitative geophysical pore-type characterization and its geological implication in carbonate reservoirs. *Geophysical Prospecting* 61:827–841. https://doi.org/10.1111/1365-2478.12043